PAPER

Hydrothermal synthesis of α-MnO₂ and β-MnO₂ nanorods as high capacity cathode materials for sodium ion batteries†

Dawei Su,[a] Hyo-Jun Ahn[b] and Guoxiu Wang*[ab]

Two types of MnO₂ polymorphs, α-MnO₂ and β-MnO₂ nanorods, have been synthesized by a hydrothermal method. Their crystallographic phases, morphologies, and crystal structures were characterized by XRD, FESEM and TEM analysis. Different exposed crystal planes have been identified by TEM. The electrochemical properties of α-MnO₂ and β-MnO₂ nanorods as cathode materials in Na-ion batteries were evaluated by galvanostatic charge/discharge testing. Both α-MnO₂ and β-MnO₂ nanorods achieved high initial sodium ion storage capacities of 278 mA h g⁻¹ and 298 mA h g⁻¹, respectively. β-MnO₂ nanorods exhibited a better electrochemical performance such as good rate capability and cyclability than that of α-MnO₂ nanorods, which could be ascribed to a more compact tunnel structure of β-MnO₂ nanorods. Furthermore, the one-dimensional architecture of nanorods could also contribute to facile sodium ion diffusion in the charge and discharge process.

1 Introduction

Li-ion batteries are considered to be the most advanced power sources for portable electronic devices and electric vehicles.[1] However, the high cost of Li-ion batteries and limited Li reserves hampered their applications for large-scale energy storage such as for renewable energy and smart electric grids. In this regard, Na-ion batteries have emerged as an alternative due to the low cost,[1,2] abundant supply (4th most abundant element in the earth's crust) and widespread terrestrial reserves of sodium mineral salts. Na-ion batteries have similar features to Li-ion batteries: non-aqueous electrolytes, alkali insertion electrodes,[3] and stable diffusion barrier of Na-ion.[4] However, the higher ionization potential[3] and larger ionic diameter of Na ((1.02 Å) *versus* Li (0.76 Å))[5] limit the structural variability and choice of Na insertion materials in crystalline materials. Therefore, finding and optimizing suitable electrode materials are crucial for the development of Na-ion batteries. So far, considerable progress has been achieved. Hard carbon materials with a large interlayer distance and disordered structure, which facilitate Na ion insertion and extraction, have been

studied as anode materials.[6–8] Alternative oxide anodes such as Na₂Ti₃O₇ (ref. 9) and TiO₂-nanotubes[10] have also been recently investigated. For cathode materials, layered oxides, NaₓCoO₂,[11] Na₂/₃(Ni₁/₃Fe₁/₃Mn₂/₃)O₂,[12] NaCrO₂,[13,14] NaₓVO₂ (ref. 15) and a new type of bi-layered NaₓV₂O₅ (ref. 16), have been investigated. However, they are all limited by either low capacity or poor cyclability. In addition, a framework material based on the phosphate polyanion, olivine NaFePO₄, has also been reported by Zaghib *et al.*[17] It demonstrated a 147 mA h g⁻¹ initial specific capacity, but its reversibility is poor (50.6 mA h g⁻¹ in the second cycle). Fluoride-based cathode materials, NaMF₃ (M = Fe, Mn, V and Ni),[18,19] have been prepared with the aim to overcome the low theoretical specific capacity of polyanionic cathodes, but they still did not achieve the satisfactory specific capacities (ranging from 30 to 170 mA h g⁻¹). Manganese oxides have large-size tunnels, which could be a potential cathode host to accommodate Na ion insertion and extraction.[20] Many previous investigations focused on sodium intercalated manganese oxide materials.[21–23] Recently, MnO₆ octahedra and MnO₅ square pyramids were found to form large, double ion channels in orthorhombic Na₄Mn₉O₁₈ (Na₀.₄₄MnO₂) and offer 130 mA h g⁻¹ capacity.[21–23] They also exhibited stable cycling performance, owing to their capability to tolerate stress during structural changes. Morales *et al.* reported that layered P2-Na₀.₆MnO₂ can deliver a 150 mA h g⁻¹ capacity in the first cycle.[20,24,25] However, this material showed a poor capacity retention with more than 50% capacity loss after only 10 cycles. Manganese dioxide has many different types of polymorphs, and all of them have large open tunnels, which can accommodate guest cations.[21,26] Therefore, they can be potentially used as cathode materials for Na-ion batteries. Herein, we report the

[a] Clean Energy Technology, School of Chemistry and Forensic Science, University of Technology, Sydney, NSW 2007, Australia. E-mail: Guoxiu.Wang@uts.edu.au; Fax: +61 2 95141460; Tel: +61 2 95141741

[b] School of Materials Science and Engineering, Gyeongsang National University, 900 Gazwa-dong, Jinju, Gyeongnam 660-701, Republic of Korea

† Electronic supplementary information (ESI) available: N₂ absorption isotherms of α-MnO₂ and β-MnO₂ nanorods, additional FESEM and TEM images of α-MnO₂ and β-MnO₂ nanorods, CV curves of α-MnO₂ and β-MnO₂ nanorods, cycle performance of α-MnO₂ nanorods, and A.C. impedance spectra of α-MnO₂ and β-MnO₂ nanorods. See DOI: 10.1039/c3ta00031a

This journal is © The Royal Society of Chemistry 2013

J. Mater. Chem. A, 2013, **1**, 4845–4850 | **4845**

synthesis, structural characterisation and electrochemical performance of α-MnO$_2$ and β-MnO$_2$ nanorods. Both α-MnO$_2$ and β-MnO$_2$ nanorods exhibited the capability for reversible Na-ion storage as cathode materials in Na-ion batteries. In particular, β-MnO$_2$ nanorods demonstrated a high capacity, good rate performance and satisfactory cyclability.

2 Experimental

2.1 Materials synthesis

α-MnO$_2$ and β-MnO$_2$ nanorods were synthesized by a hydrothermal method. For the synthesis of α-MnO$_2$ nanorods, 1.5 mmol KMnO$_4$ and 5 mmol concentrated HCl were added to 15 mL deionized water. The mixture was stirred vigorously for several minutes until a transparent purple solution was formed and then transferred into a Teflon-lined stainless steel autoclave (25 mL in capacity). The autoclave was sealed and heated to 140 °C and maintained for 12 h. To produce β-MnO$_2$ nanorods, 1 mmol (NH$_4$)$_2$S$_2$O$_8$ and MnSO$_4$·H$_2$O were dissolved in 20 mL deionized water. 0.2 g of the cationic surfactant cetyltrimethylammonium bromide (CTAB) as a soft template was added into the solution and was heated to 140 °C in a Teflon-lined autoclave for 12 h. The precipitates were cooled down to room temperature, collected by centrifugation and washed with distilled water several times. After drying at 60 °C in a vacuum oven overnight, the final products were obtained.

2.2 Structural and physical characterization

The crystal structure and phase of the as-prepared materials were characterized by X-ray diffraction (XRD, Siemens D5000) using a Cu Kα radiation at a scanning step of 0.02° min^{-1}. The morphology was analyzed by field emission scanning electron microscopes (FESEM, Zeiss Supra 55VP). The crystal structure details were further characterized by transmission electron microscopy (TEM) and high-resolution transmission electron microscopy (HRTEM, JEOL JEM-2011). Selected area electron diffraction (SAED) patterns were recorded by a Gatan CCD camera in a digital format. The specific surface areas were measured by N$_2$ adsorption isotherms using a Quadrasorb SI analyzer at 77 K. Brunauer–Emmett–Teller (BET) surface areas were calculated using experimental points at a relative pressure of $P/P_0 = 0.05$–0.25.

2.3 Electrochemical testing

The electrodes were prepared by dispersing the as-prepared MnO$_2$ nanorods (70 wt%), acetylene carbon black (20 wt%), and poly(vinylidene fluoride) binder (PVDF, 10 wt%) in N-methyl-2-pyrrolidone (NMP) to form a slurry. The resultant slurry was pasted onto an aluminium foil (1 cm × 1 cm) using a doctor blade and dried in a vacuum oven for 12 h, followed by pressing at 200 kg cm^{-2}. The mass of each electrode was around 1.4 mg. Electrochemical measurements were carried out using two-electrode coin cells with Na metal as counter and reference electrodes and a glass microfibre (Whatman) as the separator. The CR2032-type coin cells were assembled in an argon-filled glove box (UniLab, Mbraun, Germany). The electrolyte solution

was 1 M NaClO$_4$ dissolved in a mixture of ethylene carbonate (EC) and propylene carbonate (PC) with a volume ratio of 1 : 1. Cyclic voltammetry (CV) was carried out on a CHI 660C electrochemistry workstation with a scan rate of 0.1 mV s^{-1} from 1 to 4.3 V in a two-electrode system. The charge–discharge measurements were performed at ambient temperature at different current densities in the voltage range from 1 to 4.3 V. The A.C. impedance measurement was carried out on a CHI 660C electrochemistry workstation in the frequency range between 100 kHz and 10 mHz.

3 Results and discussion

Fig. 1a shows the XRD patterns of α-MnO$_2$ and β-MnO$_2$ nanorods. The product prepared using a KMnO$_4$ precursor solution was identified to be a pure α-MnO$_2$ phase (JCPDS no. 44-0141, tetragonal, $I4/m$, $a = b = 9.78$ Å, $c = 2.86$ Å), while the product prepared using a MnSO$_4$·H$_2$O precursor solution can be identified to be a pure β-MnO$_2$ phase (JCPDS no. 24-0735, tetragonal, $P4_2/mnm$, $a = b = 4.39$ Å, $c = 2.87$ Å). No impurity phases were observed, when compared to the simulated diffraction patterns of α-MnO$_2$ and β-MnO$_2$ (the black and green solid lines in Fig. 1a, respectively). In general, MnO$_2$ can form several polymorphs since the MnO$_6$ octahedral units can be linked in different ways.[27] α-MnO$_2$ is constructed from the double chains of edge-sharing MnO$_6$ octahedra that are linked at the corners to form a $(2 \times 2) + (1 \times 1)$ tunnel structure, while β-MnO$_2$ shows a 1D channel (1×1) structure composed of individual chains of
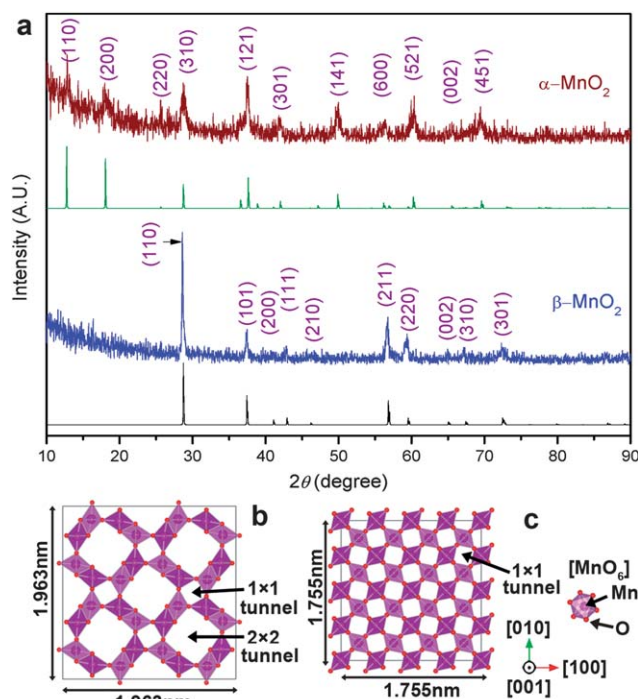

Fig. 1 (a) X-ray diffraction patterns of α-MnO$_2$ nanorods (wine in color), β-MnO$_2$ nanorods (blue in color). The black and green solid lines are simulated diffraction patterns based on the refined crystal structure of α-MnO$_2$, (b) the crystal structure of α-MnO$_2$ along the [001] direction, (c) the crystal structure of β-MnO$_2$ along the [001] direction.

the MnO_6 octahedral units as illustrated in Fig. 1b and c, respectively. The K ions, coming from $KMnO_4$, can serve as the crucial guest cations to direct the precursor to form a (2×2) tunnel structure of α-MnO_2.[28] There is no suitable guest cation in the $MnSO_4$ precursor, therefore, the small (1×1) tunnel of β-MnO_2 will be formed.[29] From the [001] projected direction of the simulated crystal structure, it can be seen that α-MnO_2 has $2 \times (1 \times 1)$ and $2 \times (2 \times 2)$ tunnels per formula unit with a tunnel density of 0.042 $\mathring{A}^{-2}$, while β-MnO_2 has $2 \times (1 \times 1)$ tunnels per formula unit with a tunnel density of 0.104 $\mathring{A}^{-2}$. Therefore, β-MnO_2 has more than twice tunnels per unit area than that of α-MnO_2. It suggests that β-MnO_2 can accommodate more Na ions. The BET specific surface areas were measured by nitrogen adsorption isotherms at 77 K (as shown in Fig. S1, ESI†). α-MnO_2 nanorods have higher surface area (33.54 $m^2\ g^{-1}$) than β-MnO_2 nanorods (14.15 $m^2\ g^{-1}$).

Both α-MnO_2 and β-MnO_2 show typical nanorod morphology with uniform size distribution. As shown in Fig. 2a and c, the low magnification FESEM images exhibit the lengths of nanorods extending to a few micrometers. Fig. 2b and d show the cross-sections of α-MnO_2 and β-MnO_2 nanorods, respectively. α-MnO_2 nanorods have a rectangle cross-section, while β-MnO_2 nanorods have a rectangle pyramid tip. Fig. S2 and S3 (ESI†) present more low and high magnification FESEM images of α-MnO_2 and β-MnO_2 nanorods, further illustrating that the as-prepared products consist of 100% 1D nanorods without any particles.

Crystal structures of α-MnO_2 and β-MnO_2 nanorods were analysed by TEM, HRTEM and SAED characterisation (Fig. 3). The individual nanorods are clearly distinguishable (as shown in Fig. 3(a_1) and (b_1), respectively). Fig. 3(a_2) and (b_2) show high magnification TEM images of a α-MnO_2 nanorod and a β-MnO_2 nanorod, respectively. Their corresponding SAED patterns are shown as insets. The dot style SAED patterns confirmed the single crystalline nature of α-MnO_2 and β-MnO_2 nanorods. For α-MnO_2 nanorod, the rhombic SAED spot pattern can be well indexed along the [111] zone axis, which indicates that the facet
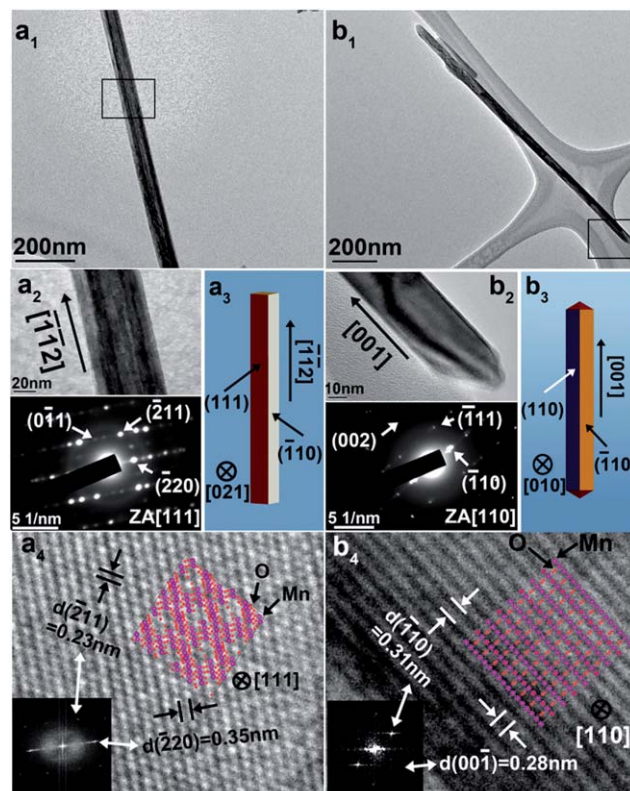

Fig. 3 Low magnification TEM images of a free standing α-MnO_2 nanorod (a_1) and β-MnO_2 nanorod (b_1). (a_2) and (b_2) are high magnification TEM images taken from rectangular regions in (a_1) and (b_1) The inset images in (a_2) and (b_2) are their corresponding selected area electron diffraction spot patterns (SAED). (a_3) and (b_3) are geometrical models of α-MnO_2 and β-MnO_2 nanorods, in which different colours present different crystal planes. Lattice resolved HRTEM images of α-MnO_2 nanorod (a_4) and β-MnO_3 nanorod (b_4). Left bottom inset images in (a_4) and (b_4) are their corresponding Fast-Fourier-Transform (FFT) patterns. The middle insets in (a_4) and (b_4) simulate the [111] projection of the tetragonal α-MnO_2 crystal structure and the [110] projection of the tetragonal β-MnO_2 crystal structure, respectively (Mn and O marked as purple and red in colour).
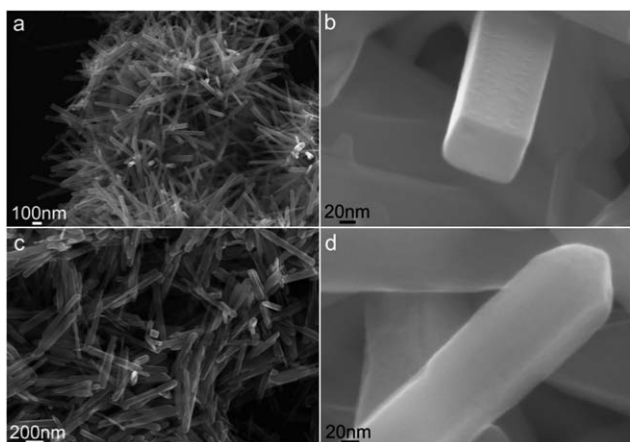

Fig. 2 (a) and (c) are low magnification FESEM images of α-MnO_2 nanorods and β-MnO_2 nanorods, respectively. (b) and (d) are high magnification FESEM images of α-MnO_2 nanorods and β-MnO_2 nanorods, showing the cross-section of nanorods.

vertical to the electron beam is the (111) crystal plane. The two side facets are the ($\bar{1}$10) and (1$\bar{1}$0) exposed crystal planes, respectively. α-MnO_2 nanorods were identified to grow along the [$\bar{1}\bar{1}$2] direction. Additional TEM images and SAED pattern of α-MnO_2 nanorods presented in Fig. S4 (ESI†) further identified the features of α-MnO_2 nanorods. Therefore, the (111) and (110) crystal planes are exposed facets along the longitudinal direction. Fig. 3(a_3) shows the geometric model of the α-MnO_2 nanorod.

Similarly, the exposed facet of the β-MnO_2 nanorod (vertical to the electron beam) can be identified as the (110) crystal plane based on the rectangle SAED spot pattern (Fig. 3(b_2)), along the [110] zone axis. β-MnO_2 nanorods grow along the (001) direction. If tilted 45° around the [001] axis, the SAED spot pattern can be indexed along the [010] zone axis (Fig. S5c and d, ESI†), indicating that the other two exposed facets of the β-MnO_2 nanorod are ($\bar{1}$10) and (1$\bar{1}$0) crystal planes. The schematic model of β-MnO_2 nanorods is presented in Fig. 3(b_3), from which it is evident that the β-MnO_2 nanorod is enclosed within the (110) and ($\bar{1}$10) crystal planes along the longitudinal

direction. The lattice resolved HRTEM images of α-MnO$_2$ and β-MnO$_2$ nanorods are shown in Fig. 3(a$_4$) and (b$_4$), respectively. Their corresponding Fast-Fourier-Transform (FFT) patterns are shown as the insets in Fig. 3(a$_4$) and (b$_4$). The FFT pattern of α-MnO$_2$ nanorods can be simulated by formula units of the tetragonal crystal structure along the [111] projected direction (presented as the inset (middle) in Fig. 3 (a$_4$)). When turned 42° along the [1$\bar{1}$0] axis, the tunnels towards the (001) crystal plane can be observed. The ($\bar{2}$11) and ($\bar{2}$20) crystal planes with 0.23, 0.35 nm lattice spacings and 58.9° interfacial angle can be directly observed. For the β-MnO$_2$ nanorod, two orthogonal crystal planes ($\bar{1}$10) and (00$\bar{1}$) with 0.31 and 0.28 nm lattice spacings were identified. The (110) crystal plane presents a rectangular atom arrangement as simulated along the [110] projected direction (middle inset in Fig. 3(b$_4$)).

Electrochemical properties of α-MnO$_2$ and β-MnO$_2$ nanorods as cathode materials in Na-ion batteries were investigated by constant charge and discharge cycling. Fig. 4 shows the voltage profiles of α-MnO$_2$ and β-MnO$_2$ nanorods at a low current density of 20 mA g^{-1} in the first and second cycles. For α-MnO$_2$ nanorods, the initial specific discharge and charge capacities are 278 and 407 mA h g^{-1}, respectively. At the second cycle, they dropped to 204 and 250 mA h g^{-1}. No obvious discharge potential plateau appeared during charge and discharge cycling. β-MnO$_2$ nanorods exhibited an initial discharge capacity of 298 mA h g^{-1} which then dropped to 240 mA h g^{-1} in the second cycle. Although the initial discharge potential plateau is not obvious, β-MnO$_2$ nanorods evolved a discharge voltage plateau between 3.0 V and 2.0 V in the second cycle. The electrochemical reaction between Na$^+$ ions and cathode hosts was further studied by cyclic voltammetry (as shown in Fig. S6, ESI†). The cathodic and anodic peaks are consistent with the charge–discharge voltage plateau. β-MnO$_2$ nanorods showed a low over-potential after the first cycle. Two

redox peaks at 2.36 and 2.66 V correspond to Na$^+$ insertion into/extraction from the β-MnO$_2$ crystal structure.[29,30]

The cycling performances of α-MnO$_2$ and β-MnO$_2$ nanorods are shown in Fig. 5. β-MnO$_2$ nanorods demonstrated a much better cyclability than that of α-MnO$_2$ nanorods. β-MnO$_2$ nanorods maintained 145 mA h g^{-1} discharge capacity after 100 cycles. However, α-MnO$_2$ nanorods only delivered a capacity of 75 mA h g^{-1} after 100 cycles. The rate capabilities of β-MnO$_2$ nanorods were also tested at different current densities (Fig. 5b). β-MnO$_2$ nanorods delivered a discharge capacity of 246 mA h g^{-1} at 50 mA g^{-1}, 188 mA h g^{-1} at 100 mA g^{-1}, and 176 mA h g^{-1} at 200 mA g^{-1} current densities. Although the specific capacity gradually decreases with increasing current density, a high initial discharge capacity (96 mA h g^{-1}) has been achieved at 400 mA g^{-1}. Even at 800 mA g^{-1}, 88 mA h g^{-1} discharge capacity was still obtained. After 100 cycles, they all stabilised at acceptable values of 93 mA h g^{-1} at 50 mA g^{-1}, 70 mA h g^{-1} at 100 mA g^{-1}, 68 mA h g^{-1} and 55 mA h g^{-1} at 400 mA g^{-1} and 800 mA g^{-1}, respectively. The rate performance of β-MnO$_2$ nanorods is much better than that of α-MnO$_2$ nanorods (Fig. S7, ESI†) and previously reported cathode materials for Na-ion batteries.[11–15,20,21,23,25] From the Nyquist plots of the A.C. impedance spectra (Fig. S8, ESI†), we can observe relatively low impedance of β-MnO$_2$ nanorods (both fresh cell and after 5
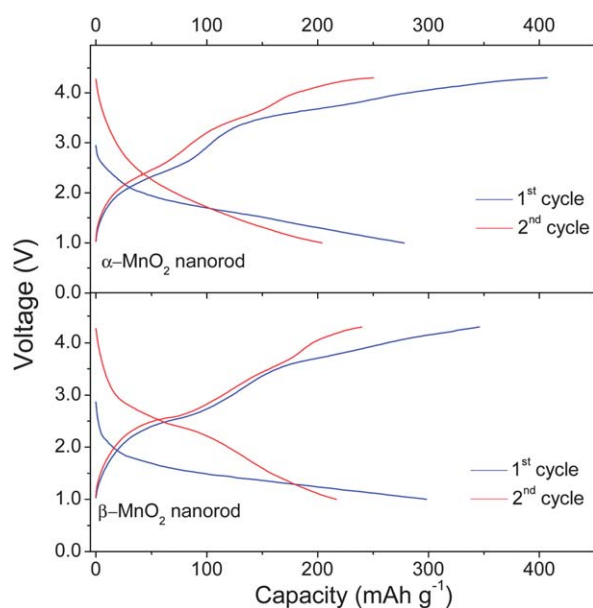

Fig. 5 (a) Cycling performances of α-MnO$_2$ and β-MnO$_2$ nanorod electrodes at a current density of 20 mA g^{-1}. (b) Discharge capacity vs. cycle number of the β-MnO$_2$ nanorod electrode at high current densities of 50, 100, 200, 400, and 800 mA g^{-1}.

Fig. 4 The discharge and charge profiles of α-MnO$_2$ and β-MnO$_2$ nanorods in the 1st and 2nd cycles. Current density: 20 mA g^{-1}.
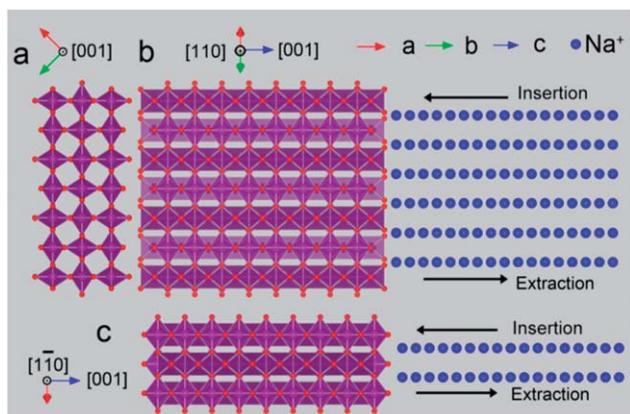
Fig. 6 Schematic illustration of the crystal structure of β-MnO$_2$ nanorods (a) along the [001] direction, (b) along the [110] direction, (c) along the [1$\bar{1}$0] direction. (b) and (c) illustrate that Na ions insert and extract in the tunnels of β-MnO$_2$ nanorods. Mn, O, and Na are colored in purple, red and blue, respectively.

cycles). Therefore, the charge transfer resistance of β-MnO$_2$ nanorods is much lower than that of the α-MnO$_2$ nanorods.

The excellent electrochemical performance of β-MnO$_2$ nanorods could be ascribed to the compact and dense (1 × 1) tunnel-structure in β-MnO$_2$ crystals. The radius of Na ion (1.02 Å) is much smaller than the size of the (1 × 1) tunnel (2.3 Å × 2.3 Å).[30,31] Therefore, Na ions can facilely insert and extract along the (1 × 1) tunnels in β-MnO$_2$ nanorods. Fig. 6 illustrates the Na ion transportation in β-MnO$_2$ nanorods. We can see that Na ions intercalate/de-intercalate in the compact (1 × 1) tunnels along the [001] direction, resulting in a high Na storage capacity and good cyclability. In contrast, the (2 × 2) + (1 × 1) two-tunnel structure in α-MnO$_2$ is not stable, inducing a low capacity and poor cyclability.[29]

4 Conclusions

α-MnO$_2$ and β-MnO$_2$ nanorods have been synthesized by a hydrothermal method. FESEM and TEM analyses confirmed the nanorod morphology and single crystalline nature of the as-prepared products. When applied as cathode materials in Na-ion batteries, β-MnO$_2$ nanorods exhibited a much better electrochemical performance than that of α-MnO$_2$ nanorods, which could be ascribed to the more compact tunnel-structure of β-MnO$_2$. β-MnO$_2$ nanorods also demonstrated a good high rate performance and durable cyclability. More specifically, β-MnO$_2$ nanorods delivered a high reversible Na ion capacity of 298 mA h g^{-1} at 20 mA g^{-1} current density. After 100 cycles, the electrode maintained a capacity of 145 mA h g^{-1}. β-MnO$_2$ nanorods could be a promising high capacity cathode material for Na-ion batteries.

Acknowledgements

Notes and references

1 J. M. Tarascon, *Nat. Chem.*, 2010, **2**, 510.

2 J. M. Tarascon, *Philos. Trans. R. Soc., A*, 2010, **368**, 3227–3241.

3 V. Palomares, P. Serras, I. Villaluenga, K. B. Hueso, J. Carretero-Gonzalez and T. Rojo, *Energy Environ. Sci.*, 2012, **5**, 5884–5901.

4 S. P. Ong, V. L. Chevrier, G. Hautier, A. Jain, C. Moore, S. Kim, X. H. Ma and G. Ceder, *Energy Environ. Sci.*, 2011, **4**, 3680–3688.

5 Y. L. Cao, L. F. Xiao, M. L. Sushko, W. Wang, B. Schwenzer, J. Xiao, Z. M. Nie, L. V. Saraf, Z. G. Yang and J. Liu, *Nano Lett.*, 2012, **12**, 3783–3787.

6 R. Alcantara, J. M. Jimenez-Mateos, P. Lavela and J. L. Tirado, *Electrochem. Commun.*, 2001, **3**, 639–642.

7 R. Alcantara, P. Lavela, G. F. Ortiz and J. L. Tirado, *Electrochem. Solid-State Lett.*, 2005, **8**, A222–A225.

8 D. A. Stevens and J. R. Dahn, *J. Electrochem. Soc.*, 2000, **147**, 1271–1273.

9 P. Senguttuvan, G. Rousse, V. Seznec, J.-M. Tarascon and M. Rosa Palacin, *Chem. Mater.*, 2011, **23**, 4109–4111.

10 H. Xiong, M. D. Slater, M. Balasubramanian, C. S. Johnson and T. Rajh, *J. Phys. Chem. Lett.*, 2011, **2**, 2560–2565.

11 R. Berthelot, D. Carlier and C. Delmas, *Nat. Mater.*, 2011, **10**, 74–80.

12 D. Kim, E. Lee, M. Slater, W. Q. Lu, S. Rood and C. S. Johnson, *Electrochem. Commun.*, 2012, **18**, 66–69.

13 S. Komaba, C. Takei, T. Nakayama, A. Ogata and N. Yabuuchi, *Electrochem. Commun.*, 2010, **12**, 355–358.

14 X. Xia and J. R. Dahn, *Electrochem. Solid-State Lett.*, 2012, **15**, A1–A4.

15 D. Hamani, M. Ati, J.-M. Tarascon and P. Rozier, *Electrochem. Commun.*, 2011, **13**, 938–941.

16 S. Tepavcevic, H. Xiong, V. R. Stamenkovic, X. Zuo, M. Balasubramanian, V. B. Prakapenka, C. S. Johnson and T. Rajh, *ACS Nano*, 2012, **6**, 530–538.

17 K. Zaghib, J. Trottier, P. Hovington, F. Brochu, A. Guerfi, A. Mauger and C. M. Julien, *J. Power Sources*, 2011, **196**, 9612–9617.

18 I. D. Gocheva, M. Nishijima, T. Doi, S. Okada, J. Yamaki and T. Nishida, *J. Power Sources*, 2009, **187**, 247–252.

19 Y. Yamada, T. Doi, I. Tanaka, S. Okada and J. Yamaki, *J. Power Sources*, 2011, **196**, 4837–4841.

20 A. Caballero, L. Hernan, J. Morales, L. Sanchez, J. S. Pena and M. A. G. Aranda, *J. Mater. Chem.*, 2002, **12**, 1142–1147.

21 F. Sauvage, L. Laffont, J. M. Tarascon and E. Baudrin, *Inorg. Chem.*, 2007, **46**, 3289–3294.

22 M. M. Doeff, T. J. Richardson and L. Kepley, *J. Electrochem. Soc.*, 1996, **143**, 2507–2516.

23 E. Hosono, H. Matsuda, I. Honma, S. Fujihara, M. Ichihara and H. S. Zhou, *J. Power Sources*, 2008, **182**, 349–352.

24 A. Mendiboure, C. Delmas and P. Hagenmuller, *J. Solid State Chem.*, 1985, **57**, 323–331.

25 R. Stoyanova, D. Carlier, M. Sendova-Vassileva, M. Yoncheva, E. Zhecheva, D. Nihtianova and C. Delmas, *J. Solid State Chem.*, 2010, **183**, 1372–1379.

26 M. M. Doeff, M. Y. Peng, Y. P. Ma and L. C. Dejonghe, *J. Electrochem. Soc.*, 1994, **141**, L145–L147.

27 J. E. Post, *Proc. Natl. Acad. Sci. U. S. A.*, 1999, **96**, 3447–3454.

28 X. F. Shen, Y. S. Ding, J. Liu, J. Cai, K. Laubernds, R. P. Zerger, A. Vasiliev, M. Aindow and S. L. Suib, *Adv. Mater.*, 2005, **17**, 805–809.

29 W.-M. Chen, L. Qie, Q.-G. Shao, L.-X. Yuan, W.-X. Zhang and Y.-H. Huang, *ACS Appl. Mater. Interfaces*, 2012, **4**, 3047–3053.

30 O. Ghodbane, J. L. Pascal and F. Favier, *ACS Appl. Mater. Interfaces*, 2009, **1**, 1130–1139.

31 W. Xiao, D. L. Wang and X. W. Lou, *J. Phys. Chem. C*, 2010, **114**, 1694–1700.

Journal of Materials Chemistry

From Wikipedia, the free encyclopedia

Journal of Materials Chemistry is a peer-reviewed scientific journal publishing original (primary) research and review articles on the applications, properties and synthesis of exciting new materials. *Journal of Materials Chemistry* is published weekly by the Royal Society of Chemistry. Since the end of 2012 the journal was not accepting new articles and its activity was split into three independent journals: Journal of Materials Chemistry A, Journal of Materials Chemistry B and Journal of Materials Chemistry C.[1]

The editor of *Journal of Materials Chemistry* is Liz Dunn.

Contents

- 1 Subject coverage
- 2 Article types
- 3 Audience (readership)
- 4 See also
- 5 References
- 6 External links

Subject coverage

Journal of Materials Chemistry publishes articles on the following topics

- Inorganic: ceramics; layered materials; microporous solids and zeolites; silicates and synthetic minerals; biogenic minerals; nanomaterials; bio-related materials; organometallic precursors for thin films/ceramics

- Organic: novel molecular solids and synthetic polymers with materials applications; polymer composites; biopolymers; biocompatible and biodegradable polymers; liquid crystals (both lyotropic and thermotropic); Langmuir-Blodgett films and self-assembled monolayers (SAMs), nanomaterials, biomaterials

- Electrical properties of materials: semi-, metallic
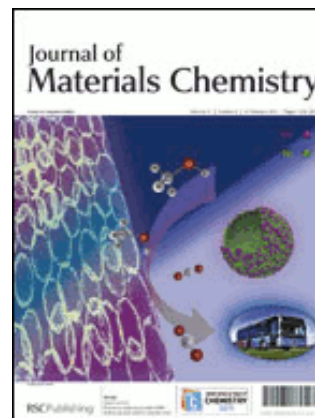
Journal of Materials Chemistry	
Abbreviated title (ISO 4)	*J. Mater. Chem.*
Discipline	Materials Science
Language	English
Edited by	Liz Dunn
Publication details	
Publisher	Royal Society of Chemistry (United Kingdom)
Publication history	1991 to 2012
Impact factor (2011)	5.968
Indexing	
ISSN	0959-9428 (http://www.worldcat.org/issn/0959-9428) (print) 1364-5501 (http://www.worldcat.org/issn/1364-5501) (web)
CODEN	JMACEP
Links	
	- Journal homepage (http://www.rsc.org/Publishing/Journals/jm/)

and super-conductivity; ionic conductivity; mixed ionic/electronic conductivity; ferro-, pyro- and piezo-electricity; electroceramics; dielectrics

- Optical properties of materials: luminescence, phosphorescence, laser action; non-linear optical effects; photoconductivity; photo- and electro-chromism, resists, glasses, amorphous semiconductors; optical modulation and switching

- Magnetic properties of materials: ferro-, ferri- and antiferro-magnetism, spin glass behaviour, organic magnetism, magnetic bubbles and information storag

- Chemical properties of materials: ion exchange, molecular separation, catalytic action, sensor action, topochemical control of reactions

- Structural properties: structural ceramics, refractories, hard materials, protective coatings, composites, adhesives, prosthetic applications

- Thermodynamic properties and phase behaviour

Article types

Journal of Materials Chemistry publishes the following types of articles: **Full Papers** (original scientific work); **Communications** (original scientific work that is of an urgent nature); **Feature articles** (reviews highlighting areas of special excitement and progress); **Highlights** (short review articles) ; and **Applications** (review articles covering the applications and properties of a class of materials). Feature articles, Highlights and Applications are written by special invitation of the Editor or Editorial Board only.

Audience (readership)

Readership of *Journal of Materials Chemistry* is interdisciplinary and includes materials scientists, chemists, physicists, ceramicists, engineers, and metallurgists

See also

- List of scientific journals in chemistry
- List of scientific journals
- Soft Matter

References

1. ^ Editorial (2013). "Journal of Materials Chemistry A, B & C – a new beginning" (http://pubs.rsc.org/en/content/articlelanding/2013/tb/c2tb90001g). *Journal of Materilas Chemistry B* **1** (1): 8. doi:10.1039/c2tb90001g (http://dx.doi.org/10.1039%2Fc2tb90001g).

External links

- Journal of Materials Chemistry (http://www.rsc.org/Publishing/Journals/jm/)
- Journal of Materials Chemistry A (http://www.rsc.org/Publishing/Journals/ta/)

- Journal of Materials Chemistry B (http://www.rsc.org/Publishing/Journals/tb/)
- Journal of Materials Chemistry C (http://www.rsc.org/Publishing/Journals/tc/)

- RSC Publishing homepage (http://www.rsc.org/Publishing/)

Retrieved from "http://en.wikipedia.org/w/index.php?
title=Journal_of_Materials_Chemistry&oldid=544530844"

Categories: Chemistry journals | Materials science journals
| Royal Society of Chemistry academic journals | Publications established in 1991
| English-language journals | Weekly journals